Aerosol Science & Technology

ISSN: 0278-6826 (Print) 1521-7388 (Online) Journal homepage: https://www.tandfonline.com/loi/uast20

Performance Evaluation of a Fiber Length Classifier

G. J. Deye , P. Gao , P. A. Baron & J. Fernback

To cite this article: G. J. Deye , P. Gao , P. A. Baron & J. Fernback (1999) Performance Evaluation of a Fiber Length Classifier, Aerosol Science & Technology, 30:5, 420-437, DOI: 10.1080/027868299304471

To link to this article: https://doi.org/10.1080/027868299304471

Published online: 30 Nov 2010.

Aerosol Science and Technology 30:420–437 (1999)

Published by Taylor & Francis, Inc.
0278-6826 / 99 / $12.00

Performance Evaluation of a Fiber Length Classifier

G. J. Deye, P. Gao, P. A. Baron, and J. Fernback
NATIONAL INSTITUTE FOR OCCUPATIONAL SAFETY AND HEALTH, CINCINNATI, OH 45226 USA (G.J.D., P.A.B., AND J.F.), NATIONAL INSTITUTE FOR OCCUPATIONAL SAFETY AND HEALTH, MORGANTOWN, WV 26505 USA (P.G.)

ABSTRACT. A performance evaluation was conducted on a differential mobility classifier that separates fibers according to length using dielectrophoresis. The classifier had been constructed and used for several applications in previous studies. The performance of the classifier was predicted using a two-dimensional axisymmetric model of the flow field and then calculating particle trajectories for a variety of conditions. Based on the flow calculations, several regions of the classifier were improved to reduce likelihood of turbulent losses. For a given total flow through the classifier and a maximum voltage across the electrodes, the performance of the classifier was found to depend on the ratios of the aerosol flow to the inner and the outer sheath flows. It was found that the minimum classifiable length, the minimum length distribution width, and the throughput of classified fibers can each be optimized, but not independently. Several approaches to testing the resolution of the classifier were tried. The first was to measure the length distribution of fibers passing through the classifier under different conditions using electron microscopy. However, this was a slow and imprecise measure of performance. Two approaches using monodisperse latex spheres were used; one operated the instrument as an electrical mobility (electrophoresis) analyzer and the other evaluated only the flow system accuracy. All measures indicate that the classifier operates close to theoretical performance, but improvements are still possible. Suggested improvements require redesign of the flow system and improved electrode alignment.

INTRODUCTION

Measurement of fiber length has been traditionally carried out using some form of microscopy. Transmission electron microscopy (TEM) is typically used for determining both length and diameter of submicrometer fibers (Baron 1993). The classification of fibers by length has been attempted by many researchers over the past 20 years. Fiber classification by inertial impaction and centrifugation followed theoretical predictions in that separation by these means was primarily dependent on physical diameter and only weakly on length (Stöber et al. 1970; Burke and Esmen 1978; Martonen 1990). Bulk fiber length classification techniques were attempted, though they did not appear to be very successful (Spurny 1980). Several researchers attempted to charge fibers and separate them according to length. Griffiths (1988) built such a device, based on earlier work by Zebel et al. (1977) and

Hochrainer et al. (1978), for use as a sampler for asbestos that would allow easier counting of long fibers. Some separation was achieved in these devices, though no further development was carried out. Greater success was achieved by charging uniform diameter carbon fibers and placing them in a standard differential mobility analyzer (Chen et al. 1993). Lipowicz and Yeh (1989) calculated the dielectrophoretic force on fibers and demonstrated that dielectrophoresis worked for aluminum fibers suspended in a liquid. They predicted that airborne fiber separation could be achieved for fibers as short as 10 μm. Lipowicz (1994) later calculated that the fiber length separation achieved by Chen et al. (1993) was largely due to dielectrophoresis rather than electrophoresis.

Based on these predictions, Baron et al. (1994) constructed a dielectrophoresis classifier that demonstrated fiber length separation. This design had a similar configuration to the Electrical Aerosol Analyzer (Model 3030, TSI, Inc., St. Paul, MN), though with smaller diameter electrodes, and was limited to collection of size-classified samples on an oiled electrode, while fibers shorter than a selected length could be retained in the aerosol phase. Further work resulted in the construction of a differential mobility classifier that allowed production of monodisperse length fibers in the aerosol phase. This device could be applied either to fiber measurement or to production of limited quantities of monodisperse fibers, e.g., for in vitro macrophage toxicity assays (Blake et al. 1997; Baron et al. 1998).

The present work describes efforts to elucidate the performance of the differential fiber length classifier. The flow field was calculated within portions of the classifier, partially to optimize the flow patterns. Also, particle trajectories based on these flow fields allowed the calculation of minimum classifiable fiber length, fiber length resolution, and classified fiber yield as a function of flow parameters. The classifier resolution and minimum fiber length were also measured experimentally and compared to the predictions.

Classifier description

The physical principles of dielectrophoretic separation used in the differential fiber length classifier operation have been described elsewhere (Lipowicz et al. 1989), so only a brief overview will be given here. Conductive fibers placed in an electric field are aligned parallel to the electric field because of fiber polarization (Lilienfeld 1985). When the field exhibits a gradient, the fiber end closest to the high field electrode will experience a larger force than the other fiber end, and the net force on the fiber will result in motion toward the higher field region. The classifier configuration consists of two concentric tubular electrodes with the highest electric field existing at the surface of the inner electrode. Conductive fibers placed in a gradient electric field will be attracted to the inner electrode with a velocity approximately proportional to the length squared. In the classifier described here (Figure 1), dielectrophoretic separation takes place primarily between two concentric tubes over a length of 76 cm. Some dielectrophoretic and gravitational motion of the fibers occurs in the flow combination section. Fiber behavior in this region is discussed below.

The classifier's overall flow system was designed to introduce an annular aerosol flow surrounded by clean humidified air to the classifier region (Figure 2). Two sheath flows (Q_{S1} and Q_{S2}) and the input aerosol flow (Q_{Aer}) were combined at the top of the classifier to form Q_{total}, the total flow in the classifier region; this flow was split apart at the bottom of the classifier, one part containing the narrow length distribution (Q_{Class}) and the other part containing the short fiber fraction (Q_{Dump}), which was normally thrown away. Typical operating flow rates of the classifier were as follows: Q_{Total} was in the range of 5–10 L/min; Q_{Aer} was 10–20% of Q_{Total}; Q_{Class} was 10–30% of Q_{Total}. The flows within the classifier were recirculated to keep the humidity and temperature constant in the classifier. Diaphragm pumps (Model 44XR, SKC, Inc., Eighty Four, PA) induced the flows and combinations of filters (as flow resistance ele-

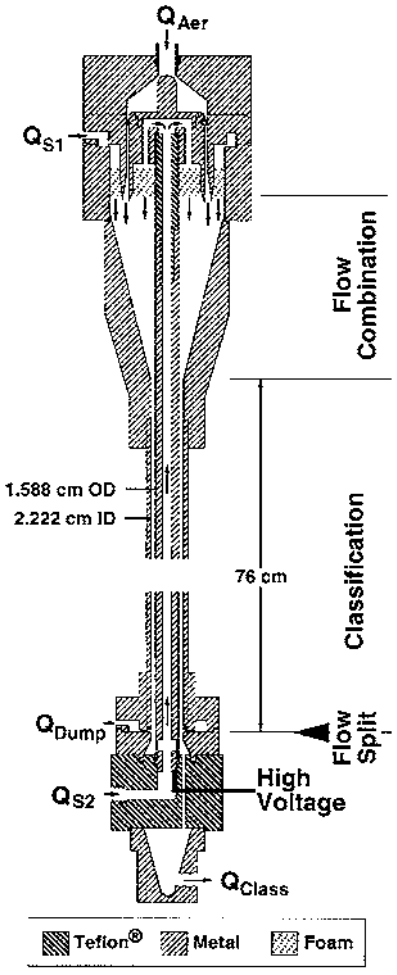

FIGURE 1. An approximate scale drawing of the fiber length classifier.

ments), and pulsation dampeners reduced pulsation within the classifier. The filters also ensured particle-free air for the sheath flows.

Q_{Aer} initially passed through a constriction to make the annular aerosol stream uniform about the axis of the classifier. Then, on entering the flow combination region, Q_{Aer} was surrounded by an outer (Q_{S1}) and an inner (Q_{S2}) sheath flow. The inner sheath flow was introduced at the bottom of the classifier and passed up through the center electrode. Both sheath flows were passed through 50 pore-per-inch open pore foam to provide uniform flow in the flow combination region. The combined flows were funneled into a narrow annular region (76 cm long) where classification took place. Longer fibers deposited on the inner electrode more rapidly than shorter ones; fibers that were pulled near the inner electrode but had not deposited were removed in the classified flow (Q_{Class}) at the bottom of the classifier. The short fibers not sufficiently attracted to the inner electrode were pulled through a slot in the outer electrode into what was termed the dump flow (Q_{Dump}). The dump slot was sufficiently narrow to ensure uniform flow in all radial directions.

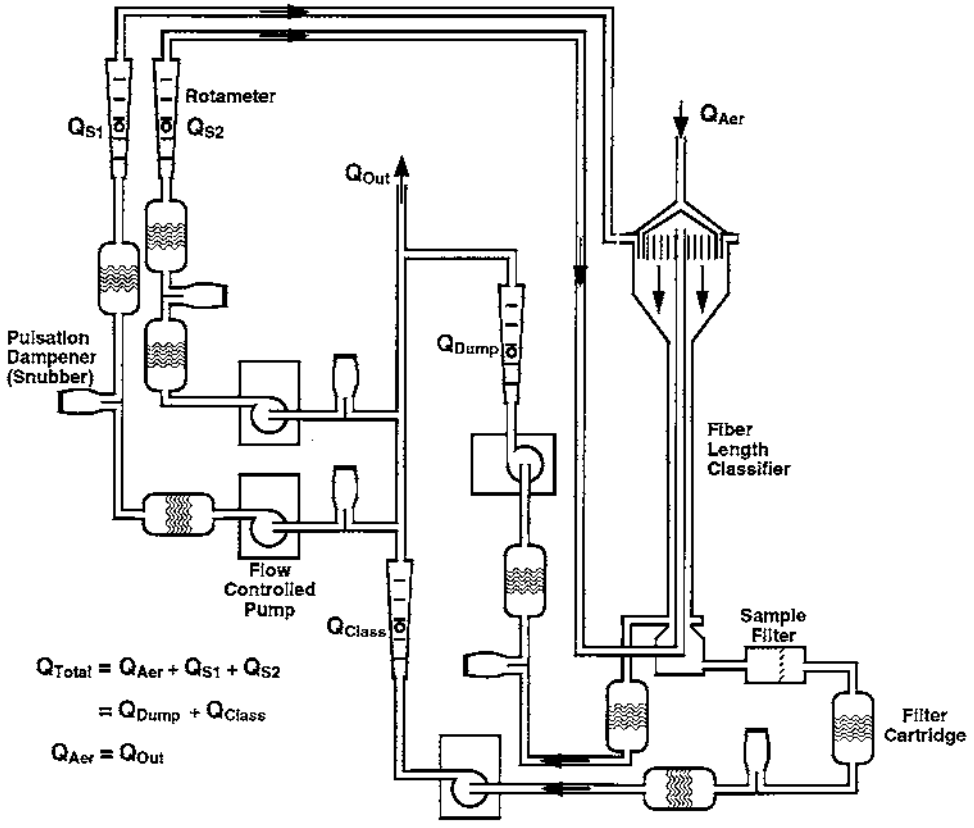

FIGURE 2. Fiber length classifier flow system.

The flows must be stable throughout to prevent mixing of the aerosol and sheath flows. The pressure variation in the flow combination region was monitored using an electret microphone attached to an oscilloscope. Unless kept to a minimum, pressure pulsation from sources outside the classifier, such as the pumps and the aerosol generator, were found to affect the length distribution spread of the classified fibers.

Fibers that deposited on the inner electrode were trapped in a nonconducting layer. This layer was important because on a clean metal electrode, the fibers deposited perpendicular to the surface and either became focal points for additional fiber deposition through a modified electrical field or resuspended and disturbed the trajectories of other fibers. All metal surfaces within the classifier where fibers might deposit, even the outer electrode, were coated with a thin grease and oil mixture to prevent these problems. The coating layer had to be nonconducting, be sufficiently viscous to prevent sagging or running, and have a low surface tension to trap fibers.

The length of the classified size fraction exiting the end of the classifier was varied by changing the voltage; however, it could also be varied by changing Q_{Total}. Typically, the voltage was set at a selected value between zero and about 7000 V. The spacing between the two electrodes was only about 3.2 mm, so the electrical breakdown of air imposed an upper voltage limit in the operation of the classifier. To reduce electrophoresis, which was greater than

dielectrophoresis for highly charged particles, the aerosol net charge was neutralized using a ^{85}Kr source prior to introduction of the aerosol to the classifier. In addition, the high voltage was applied as a bipolar 50 Hz square wave by feeding the output of a signal generator (0–10V) through a high voltage amplifier with a gain of 1000 (Model 609A-3, Trek, Inc., Medina, NY). The voltage was carefully balanced so that the wave form was centered at ground voltage within 0.5% of peak voltage; the root mean square voltage was used for calculating fiber classification. In this alternating field, charged fibers oscillated about the trajectory predicted for dielectrophoretic motion (Han et al. 1994). If the fibers were not highly charged, the oscillation was sufficiently small that additional deposition and hence significant broadening of the classified fiber distribution did not occur.

Finally, the fibers must be polarizable for dielectrophoretic separation to occur. In practical terms, the time constant for charges within the fiber to migrate the length of the fiber must be small compared with the alternating electric field period. The largest component of fiber polarizability is generally due to surface conductivity and this conductivity can be increased in the presence of atmospheric water (Lilienfeld 1985). Measurements with chrysotile asbestos fibers indicate that these fibers appear sufficiently conductive even at very low humidity levels (< 5% relative humidity (RH)), but glass fibers must be humidified to greater than 60% RH to create a conductive surface layer. Humidity was measured using a model HMI 32 hygrometer (Vaisala Instruments). Fiber measurements were made at > 70% RH to ensure fiber polarizability.

THEORETICAL

Flow field

The primary problems in accurate fiber classification were assumed to occur in regions where flows were being combined or split apart. Therefore, the flow field was calculated in the flow combination region where aerosol is introduced to the classifier and in the flow split region at the end of the classifier. In the classification region the flow velocity profile was close to a parabolic profile and was calculated in closed form (White 1986).

The flow fields within the classifier were calculated using an axisymmetric two-dimensional computational fluid dynamics (CFD) model. The model calculations were carried out with a finite- element method using a commercially available software package (FIDAP, version 7.61, Fluent Inc., Lebanon, NH). Because inclusion of the classifier region would make the model larger and would not provide additional important information, the simulations were carried out in two separate numerical models, i.e., one for the flow combination region at the inlet and the other for the flow split region at the bottom of the classifier (see Figure 1).

The mesh for the flow combination region was determined by 6,570 nodes. In the flow split region, the mesh contained 3,581 nodes for the current design, while 3,800 nodes were used for an improved version in which an insert was made out of teflon® to optimize the flow pattern. To ensure a grid-independent solution, the number of nodal points was uniformly increased throughout the computational domain of the flow combination region by a factor of four. A comparison at a 10 L/min total flow and 1 L/min aerosol flow for a 0.35 μm diameter by 7.0 μm long glass fiber showed that the predicted mean length was changed only by 0.18%. Hence, the lower density of the computational mesh was considered adequate to calculate the flow field, and subsequent calculations for the various flow conditions were conducted at the lower mesh density.

The initial flow velocity in the inlet of the flow combination region was described by a parabolic profile as expected. Based on the closed form (White 1986), the flow velocity profile in the downstream of the classifier region was calculated to be close to a parabolic profile with its maximum slightly closer to the inner electrode, i.e., a ratio of 0.47 was obtained ver-

sus a ratio of 0.50 while at the midpoint. A parabolic profile, in turn, was chosen to specify the initial flow velocity of the flow split region.

The velocity components in the radial and axial direction at various flow conditions directly solved with FIDAP were output as text files. The flow field used in the calculation of particle trajectories was a combination of the flow field calculated from the velocity filed of the axisymmetric two-dimensional models of the flow combination region and the closed form velocity profile in the classification region.

Particle trajectories

A program was written in the C language (Microsoft, Redmond, WA) to calculate particle trajectories in the classifier to estimate particle penetration under various voltage and flow conditions. The flow field determined above was used for these calculations. Particles introduced at the beginning of the flow combination region were tracked through the classifier at small time increments to determine if they reached the classified fiber flow at the end of the classifier. If the particles followed the air streamline closely, i.e., the radial velocity due to dielectrophoretic force was small, the time interval was increased to decrease the calculation time. For fibers, dielectrophoretic and gravitational forces were included, while for spherical particles only the electrophoretic forces were calculated.

The dielectrophoretic velocity (v) of fibers in a gradient electric field was calculated using the equation developed by Lipowicz and Yeh:

$$v = \frac{K_m \epsilon_0}{36\eta} dl \left\{ g(\beta) \left(\frac{\alpha}{\alpha - 1} - f(\beta) \right) \right\}^{-1} \nabla(E^2), \tag{1}$$

where d and l are the fiber length and diameter, β is the aspect ratio, f and g are complex functions of β, E is the electric field, α is the dielectric constant of the fiber, ϵ_0 is the permittivity of vacuum, K_m is the dielectric constant of air, and η is the viscosity of air. α was assumed to be large for conductive fibers. For conductive fibers, the calculated velocity was very nearly proportional to the fiber length squared and the electric field squared.

The electrophoretic velocity for a spherical particle of diameter d_p was determined from

$$V_{elec} = \frac{neE\,C_c}{3\pi\eta d_p}, \tag{2}$$

where n is the number of electronic charges (e) and C_c is the slip correction factor.

The gravitational settling of fibers in the flow combination region was included based on aerodynamic diameter:

$$d_{ae} = d\sqrt{\frac{\rho_f \beta}{\rho_0 \chi}}, \tag{3}$$

where the shape factor χ depends on the orientation of the fiber relative to the direction of gravity (Kasper 1982):

$$\chi_{\parallel} = \frac{4(\beta^2 - 1)}{3 \Big/ \left\{ \frac{2\beta^2 - 1}{\sqrt{\beta^2 - 1}} \ln\left(\beta + \sqrt{\beta^2 - 1}\right) - \beta \right\}} \tag{4}$$

$$\chi_{\perp} = \frac{8(\beta^2 - 1)}{3 \Big/ \left\{ \frac{2\beta^2 - 3}{\sqrt{\beta^2 - 1}} \ln\left(\beta + \sqrt{\beta^2 - 1}\right) + \beta \right\}}. \tag{5}$$

The orientation of the fiber at each location was calculated based on the direction of the electric field at that point.

EXPERIMENTAL

Three approaches were used in an attempt to find a way to rapidly and accurately assess the performance of the fiber length classifier. These approaches had various advantages and disadvantages. The first approach involved measurement of the output of the classifier for a range of conditions using filter collection of the fibers and mea-

surement of the fiber dimensions by TEM. The second approach involved operating the classifier with the electric field off and with normal input flows, but varying the flow split at the end of the classifier to effectively scan the penetration in the radial direction (split flow technique). The third approach involved using the classifier as an electrical mobility classifier by introducing monodisperse latex spheres (0.8 μm) into the outer sheath flow and observing the penetration as a function of DC voltage.

TEM analysis

Samples of fibers were obtained for four nominal lengths of fibers, 6, 10, 20, and 30 μm, based on earlier calibration of the classifier. The challenge aerosol presented to the fiber length classifier was ball-milled glass fibers (Insulate III, Certainteed Corp) produced from a Pitt III generator (Weyel et al. 1984) using sonic fluidization. The air passing through the generator was initially humidified to 30% RH to increase output and decrease fiber charge levels (Baron and Deye 1990). The fibers were classified with a two-stage virtual impactor prior to introduction into the fiber length classifier so that most of the fibers had diameters in the range of 1–4 μm. Q_{Total} in the fiber length classifier was 9 L/min, while Q_{Aer} was 1 L/min. The fibers were humidified to greater than 70% RH, passed through a 10 mCi ^{85}Kr radioactive source, and introduced into the fiber length classifier. The fibers were collected from the classified flow onto mixed-cellulose-ester filters. The fiber samples were prepared by direct transfer to TEM grids and analyzed (Model EM420, Philips, Holland). Approximately 300 fibers were counted for each sample.

Split flow technique

Latex particles (0.8 μm diameter) were generated from water suspension and passed near a ^{210}Po radioactive source to neutralize the total aerosol charge. The voltage in the classifier was off. The flow at the bottom of the classifier was split using the system indicated in Figure 3. The total flow through the classification region ($Q_{\text{Total}} = Q_{\text{Dump}} + Q_{\text{Class}}$) remained constant, while the measured aerosol flow was varied by adjusting the pump that produced the flow Q_{var}. The flow rate into the Aerodynamic Particle Sizer (APS3310, TSI, Inc., St. Paul, MN) was a constant 5 L/min and diluted the $Q_{\text{Class}} + Q_{\text{var}}$ that was measured. This dilution factor was corrected in the final estimate of measured concentration at the exit of the classifier. The shape of the particle count curve as a function of measured flow was a measure of whether or not the aerosol stream remained well defined as it passed through the entire classifier.

Electrical mobility technique

This approach involved operating the classifier in the more familiar mode of electrophoretic separation and measuring the mobility of spherical particles carrying one to several electrical charges. Latex particles (0.8 μm) were generated from water suspension using a nebulizer, neutralized with a ^{85}Kr source, and introduced into the outer sheath flow of the classifier. A spacer was placed in the flow combination region, reducing the outer diameter of the flow combination region so that the outer sheath flow area was 10% of the total cross-sectional area of the flow combination region. Thus, when the aerosol flow, 10% of total, was fed into the outer sheath, the velocities of the three flows in the flow combination region were equal. The voltage applied to the electrodes was a DC voltage that varied from zero to the maximum (about 7000 V). The particle count in the classified flow (Q_{Class}) was plotted as a function of voltage.

RESULTS AND DISCUSSION: THEORETICAL

Flow field

The flow field calculations resulted in a series of velocity profiles and streamline contours for

both the flow combination region at the inlet and the flow split region at the end of the classifier. An initial concern regarding the flow field combination region was that the low velocity resulted in mixing that was not damped out adequately. However, the low Reynolds number (< 250) and the fact that the flows combined in a converging cone appeared to ensure that no mixing or recirculation occurred. This was confirmed by the CFD model (Figure 4).

The flow split region at the bottom of the classifier was suspected of causing several problems. Fiber deposits were found at the downstream edge of the exit (dump) slot. The CFD calculations showed, especially at a higher flow rate of $Q_{\text{Total}} = 9$ L/min, that a stagnation point was formed downstream of the exit slot as indicated by the arrow in Figure 5a. This apparently resulted in excess impaction of fibers in this region. Deposition in this region was especially problematic during production of relatively large quantities of fibers because the deposits could break away from the vertical surface and end up in the classified flow. In addition, the CFD model indicated the presence of a recirculation region indicated by **A** in Figure 5a. To reduce these problems, a teflon® insert was placed as indicated in Figure 5b. The effect of this insert was to direct the flow toward the exit slot. This channeled the flow more smoothly into the exit slot and eliminated the flow recirculation region downstream of the slot. The stagnation point was moved to the bottom edge of the exit slot so that excess short-length fibers would not be as likely to deposit on the vertical wall of the classifier.

Particle trajectory calculations

Particle trajectories were calculated using the flow field for a number of flow conditions. A uniform distribution of particles was assumed

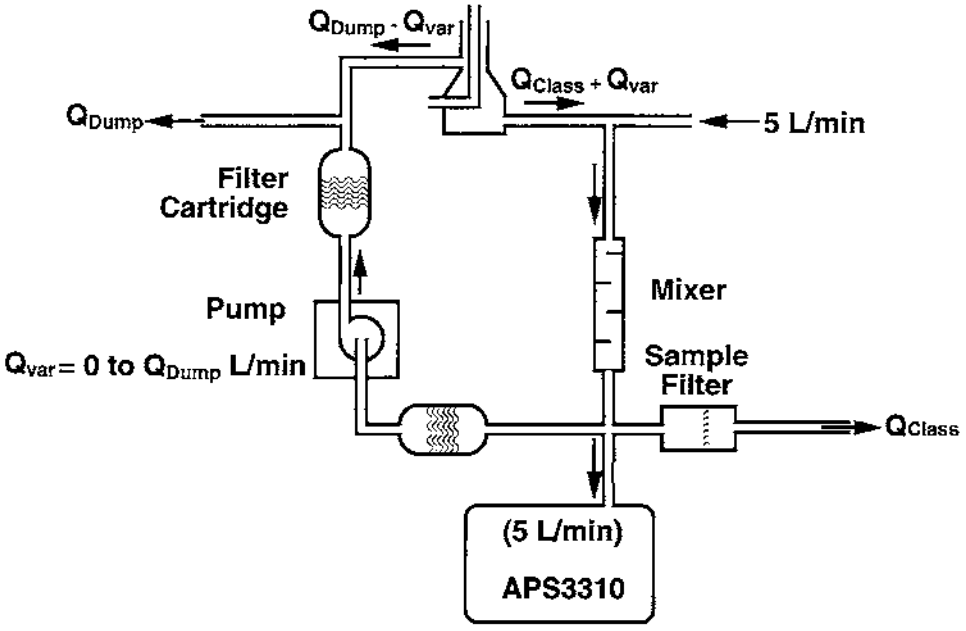

FIGURE 3. Flow system for split flow technique. The total flow through the classifier remains constant while the proportion between the classified flow and the dump flow is varied by changing Q_{var}.

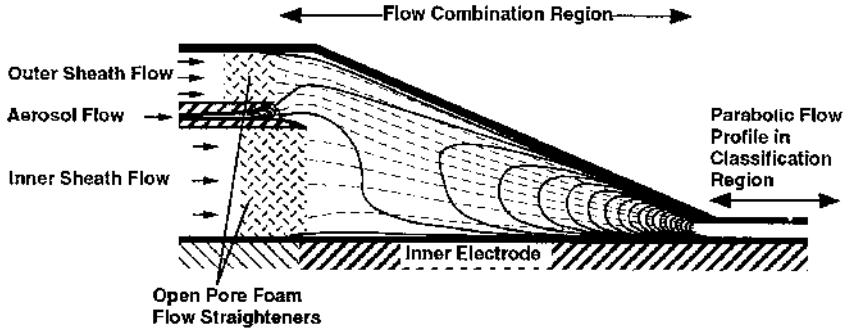

FIGURE 4. Flow pattern in flow combination region. The dashed lines are streamlines while the solid lines are velocity contours.

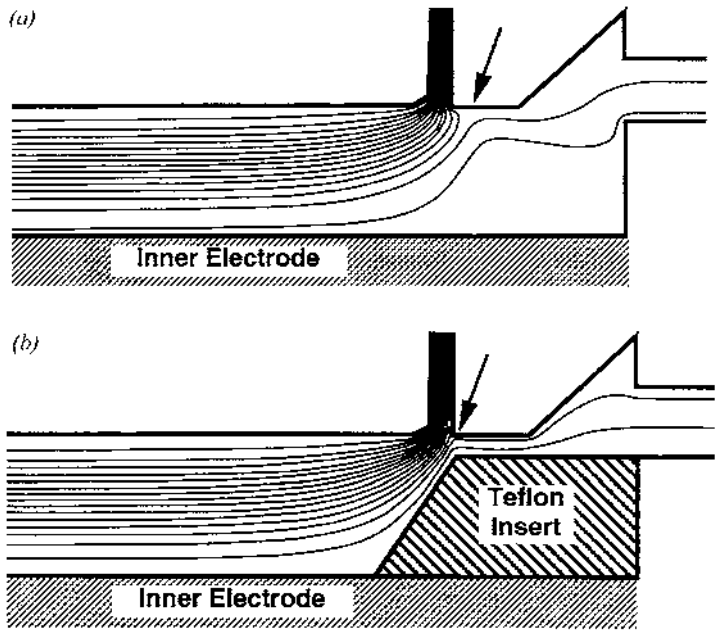

FIGURE 5. a) Calculated streamlines for 9 L/min total flow. The stagnation point downstream of the dump slot is displaced from the bottom edge of the dump slot as indicated by the arrow. This displacement allows impaction of fibers on this downstream surface. Region A also appears to exhibit a recirculation pattern. The radial dimension is exaggerated. b) Calculated streamlines for 9 L/min total flow. With the insert in place, the stagnation point downstream of the dump slot is at the bottom edge of the dump slot (arrow). This suggests reduced likelihood of impaction downstream of the dump slot. The radial dimension is exaggerated.

to fill the input aerosol flow. The fiber fraction penetrating the classifier was calculated for each of a series of conditions for fiber diameters between 0.03 and 3 μm and lengths between 3 and 300 μm. Three properties of the classifier fiber penetration were calculated. The mini-

mum fiber length that could be achieved was of interest because this defined the lower end of the range of fiber classification. The spread of the classified length distribution was represented by the calculation of the coefficient of variation (CV) of lengths reaching the classified flow. While it was recognized that the output distribution was not a normal distribution and was likely in some circumstances to be skewed, the CV offered a simple measure of the narrowness of the distribution. Finally, the relative quantity of fibers (or yield) reaching the classified flow was calculated.

To simplify the discussion, these three classifier properties are shown in Figures 6, 7, and 8 only for an input aerosol flow of 1 L/min and a total flow of 10 L/min, respectively. Other aerosol flows and total flows were calculated, but did not reveal any additional significant features. As the aerosol flow is introduced closer to the inner electrode, i.e., the inner sheath flow is smaller, a smaller minimum fiber length can be classified. However, Figure 7 indicates that when the inner sheath flow is reduced, the CV or length spread is increased. There is thus a tradeoff between minimum length and length spread in the classified distribution. The throughput has a very similar functional dependence on inner sheath flow rate as the CV. This means that at a specified minimum length, the throughput will be determined by the maximum acceptable CV.

For a classical electrophoresis classifier, the usual operating condition is to set the output sample flow equal to the input aerosol flow ($Q_{\text{Class}} = Q_{\text{Aer}}$). In this case, if Q_{Class} is less than Q_{Aer}, then no improvement in resolution is gained. However, with the dielectrophoresis classifier, the fiber motion is a function of the fiber length squared. Therefore, as Q_{Class} increases relative to a fixed Q_{Aer}, the distribution spread (as indicated by the CV) does not increase in proportion to the output flow. The curves in Figure 7 are plotted as a function of inner sheath Q_{S2}. The magnitude of inner sheath flow indi-

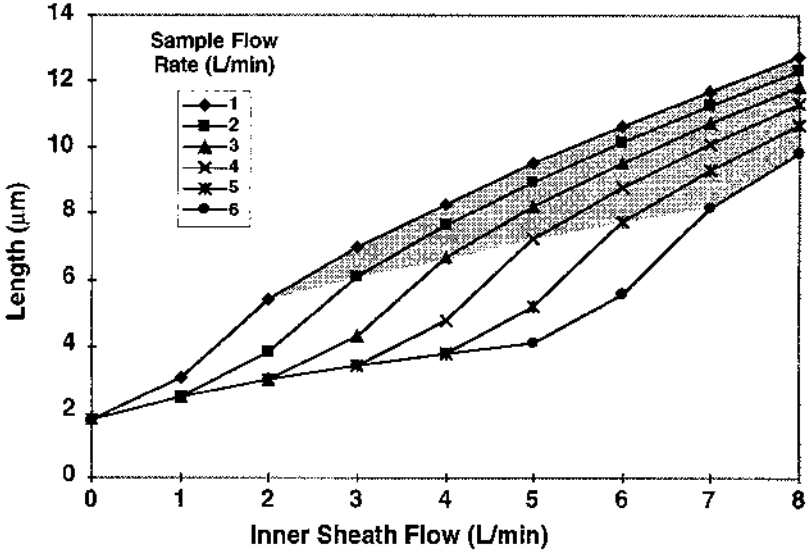

FIGURE 6. Classified length as a function of inner sheath flow (a measure of initial aerosol distance from inner electrode) at several output aerosol flow rates. Conditions: 10 L/min total aerosol flow, 1 L/min inlet aerosol flow, 6000 V_{rms}.

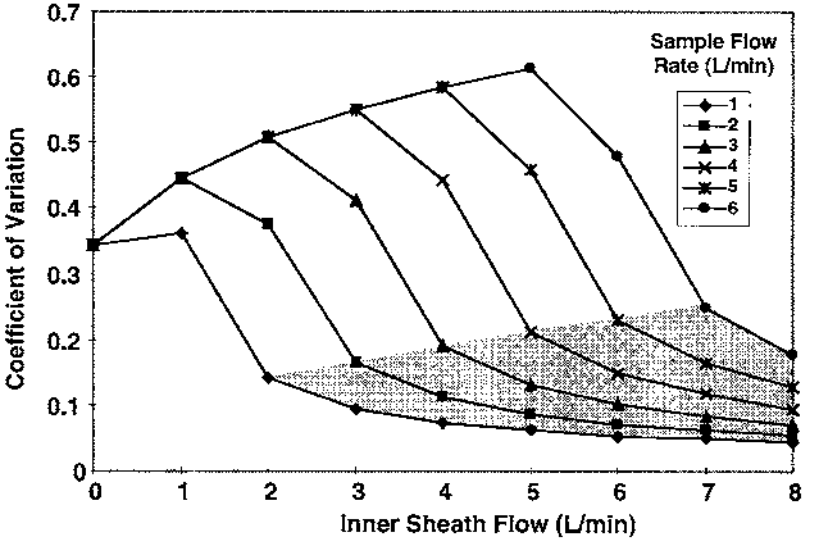

FIGURE 7. Length distribution CV as a function of inner sheath flow (a measure of initial aerosol distance from inner electrode) at several output aerosol flow rates. Conditions: 10 L/min total aerosol flow, 1 L/min inlet aerosol flow, 6000 V_{rms}.

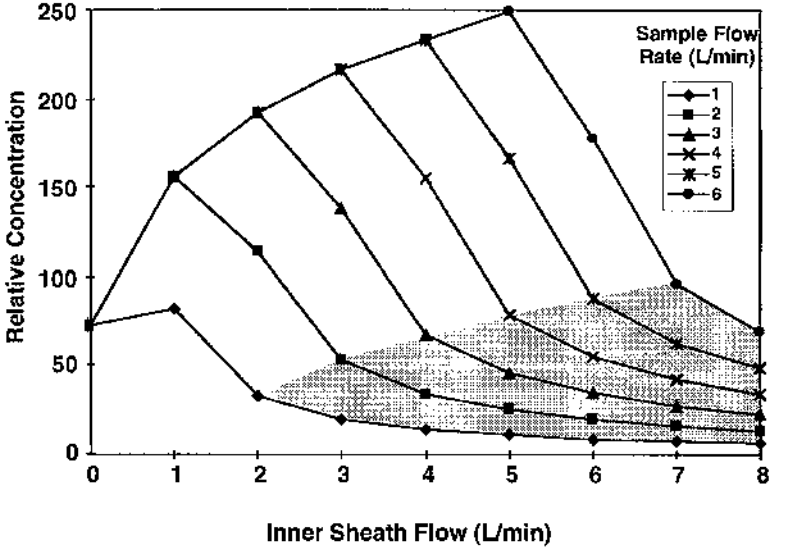

FIGURE 8. Relative yields as a function of inner sheath flow (a measure of initial aerosol distance from inner electrode) at several output aerosol flow rates. Conditions: 10 L/min total aerosol flow, 1 L/min inlet aerosol flow, 6000 V_{rms}.

cates how close to the inner electrode the aerosol is injected into the classifier. The several curves in each figure represent results for several values of the output sample flow Q_{Class}. At $Q_{S2} = 4$ L/min and at $Q_{\text{Aer}} = 1$ L/min, which are normal operating parameters of the classifier, increasing Q_{Class} from 1 to 2 L/min only increases the CV by 50%. Thus, because the fibers are separated as the square function of the length, there is no fixed optimal relationship between the two; the user must select the resolution and throughput based on the operating curves.

The curves in Figures 6, 7, and 8 all exhibit a change in slope under the flow conditions when there is about a 1 L/min offset between the inner streamline of the input aerosol flow and the outer streamline of the classified flow. For example, consider the case when the streamline marking the inner radius of the input aerosol flow passes through the classifier and is immediately adjacent to the streamline entering the outer edge of the classified flow. Then the CV is significantly larger (by about a factor of two) than if there is at least 1 L/min of sheath flow between these two streamlines. When this offset is less than 1 L/min, then a significant portion of the challenge aerosol distribution can be transferred directly into Q_{Class}, increasing the spread of the classified distribution. The useful operating region thus requires this minimum offset and is indicated in Figures 6, 7, and 8 by the shaded areas.

If one is not interested in classifying the shortest possible fibers, there is an advantage to operating the classifier with the input aerosol injected at a larger radius, i.e., larger Q_{S2}. Under this condition, one can then optimize either resolution by using a small classified aerosol flow or throughput by increasing the output aerosol flow. However, some outer sheath flow is necessary to minimize deposition on the outer electrode. Deposits on this electrode can build up quickly, resulting in disruption of both the flow field and the electric field.

Several other issues were addressed using the CFD/particle trajectory calculations. The converging flow combination region provided an opportunity for large particles to settle prior to entering the classification region. These particles had only a limited time to settle through the outer sheath flow to reach a nonvertical surface. At a 10 L/min total flow, 1 L/min aerosol flow, and 4 L/min outer sheath flow, a 15 μm diameter by 50 μm long glass fiber ($d_{ae} \approx 43$ μm) just reached the surface of the convergence cone before the classification region. Considerable improvement in the inlet section will be needed to let such large d_{ae} fibers enter the classifier, so this settling is unlikely to be a significant problem. However, even without reaching the outer electrode, the fibers can settle into the outer sheath flow thus slightly reducing the final classification resolution.

RESULTS AND DISCUSSION: EXPERIMENTAL

TEM analysis

The length and width of fibers were measured by TEM. The results are indicated in Figure 9. The fiber length means were determined from the principal mode of the distribution since the measurements included some short fibers that may have been dislodged during sample preparation. This short fiber fraction was also seen previously (Baron 1994) and attributed to an artifact of sample preparation for TEM analysis since many fiber agglomerates as well as single fibers are generated and classified. These agglomerates can break apart during sample preparation and be counted separately.

The challenge fiber distribution generated from the acoustically fluidized bed was sampled and measured by TEM. For the 1100 fibers counted, the geometric mean length was 6.5 μm ($\sigma_g = 2.5$) and the geometric mean diameter was 0.35 ($\sigma_g = 2.8$) with the correlation between length and diameter $\tau = -0.13$.

The mean length of fibers in the range from 6 μm to 30 μm agreed well with the previous calibration as indicated by the slope of the regres-

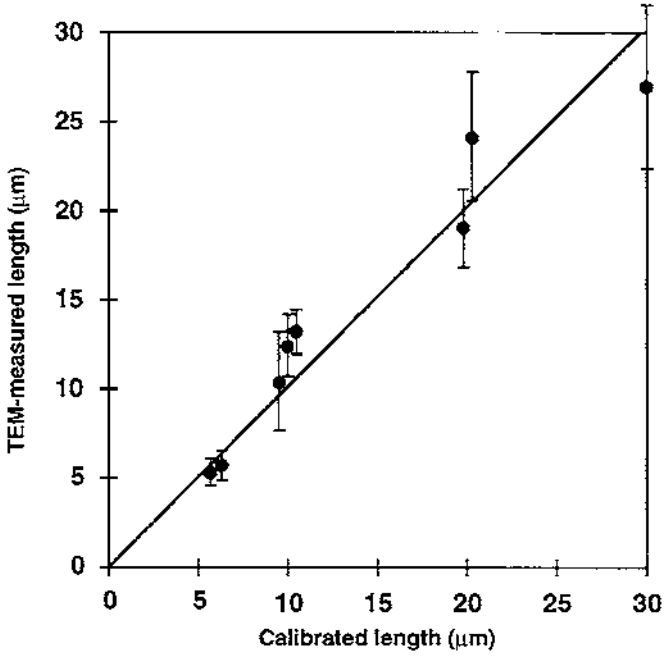

FIGURE 9. Comparison of TEM measured fiber length for classified fibers according to a previous calibration. The indicated error bars represent one standard deviation. The regression forced through zero had a slope of 1.01 with $r^2 = 0.98$. Overlapping points are displaced horizontally a small distance for visibility.

sion line (1.01; $r^2 = 0.98$), which was forced through zero. However, the deviations from the regression line averaged 14% and were as large as 32%. Part of these deviations may be due to the imprecision and biases in the TEM analysis. Counting a limited number of fibers, sample preparation and operator interpretation of fiber shapes all contribute errors to the analysis. It is difficult to assess these errors since an independent means of fiber measurement has not been available. In addition, one TEM analysis typically requires at minimum several days to complete. Therefore, other means of assessing the classification accuracy were sought.

The mean CV for all the length classified fibers measured was 0.15. This corresponded to a theoretically predicted CV of approximately 0.08. This indicated that the spread of the distribution was about twice that theoretically expected. While some of the additional spread may have been due to imprecision in the TEM analysis, measurements indicated below suggest that other factors contributed to a greater degree.

The point for 30 μm fibers lies below the regression line in Figure 9. While not statistically significant, this trend was noted on several occasions and suggested that longer fibers may not behave as theoretically predicted for fully conductive fibers. The fiber length may contribute to a larger time constant for charge equilibrium within the fiber during exposure to the alternating electric field. This may in turn contribute to a lower dielectrophoretic drift velocity. Further experiments are needed to confirm this hypothesis.

Split flow technique

Examples of the penetration curve and the extracted differential plot are shown in Figure 10. The penetration curve is an indication of particle concentration in the measured flow ($Q_{\text{Meas}} = Q_{\text{Class}} - Q_{\text{var}}$). If there is no mixing between the sheath flows and the aerosol flow and the classifier is perfectly axially symmetric, the penetration curve should be three straight lines: zero

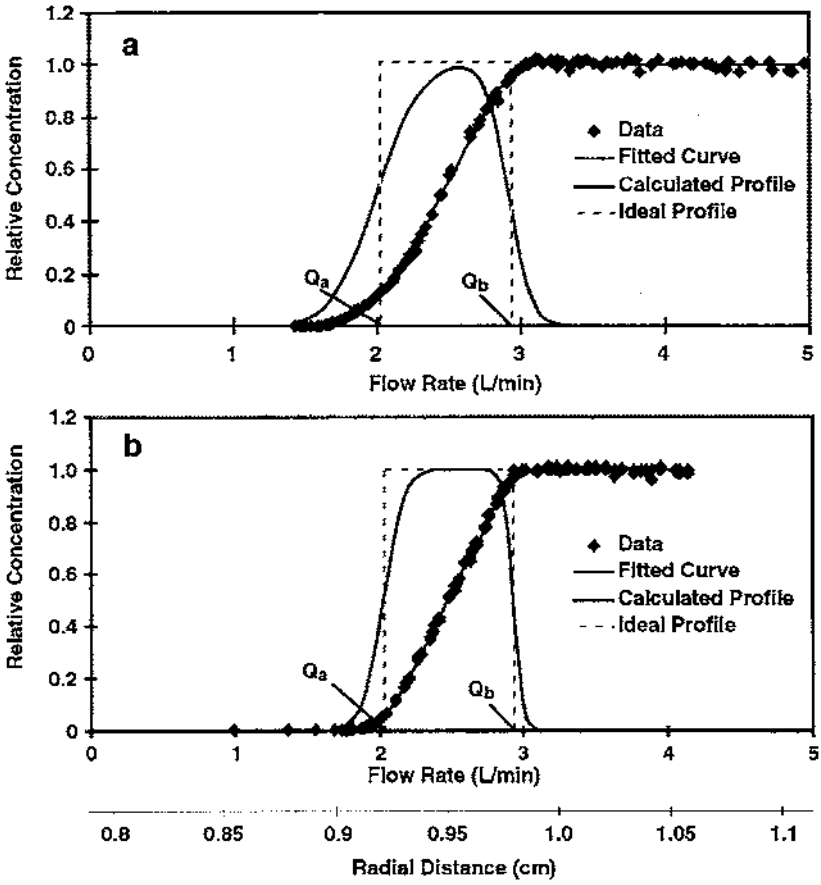

FIGURE 10. Split flow penetration curves. These curves provide an estimate of flow accuracy through the entire classifier. a) Original penetration with curved inner electrode, (D_a = 0.031, D_b = 0.0083). b) Improved (straighter) inner electrode (D_a = 0.0073, D_b = 0.0016). The curved electrode apparently caused mixing of sheath and aerosol flows, primarily near the inner electrode.

for flows below $Q_a = Q_{S1}$, an increasing linear function from zero to 1 in the region between Q_a and $Q_b = Q_{S1} + Q_{\text{Aer}}$, and 1 above Q_b. When differentiated, this ideal penetration curve results in a rectangular profile as indicated in Figure 10b. Diffusion-like dispersion terms were added centered at the breakpoints at Q_a and Q_b to simulate any mixing or asymmetry that might occur in the system, thus resulting in a less sharply defined aerosol stream. For instance, in the range from 0 to Q_a, the additional mixing term M is calculated using the error function

$$M = \frac{2}{\sqrt{\pi}} \int_o^z e^{-t^2}\, dt, \quad \text{where} \quad z = -\frac{|Q_a - Q_i|}{2\sqrt{D}}, \tag{6}$$

t is a dummy variable, and D is a diffusion term. The M term is applied piecewise to the four ranges of data: below and above Q_a, below and above Q_b. M was calculated for each flow rate

Q_i for which a particle count was obtained. The value of M was fitted to the data to minimize the least squares difference by varying the values of Q_a, Q_b, D_a, and D_b, where D_a and D_b are the dispersion terms describing mixing of aerosol about the values of Q_a and Q_b, respectively.

Using this model, the particle count data were fitted using a least squares criterion and the fitted curve was differentiated to give the original aerosol profile. The ideal aerosol profile is rectangular as described above. Curvature near the interface between the aerosol flow and the sheath flows indicates either mixing or asymmetry in the system. The results of two such calculations are presented in Figure 10. The data from the initial measurement (Figure 10a) indicate a poor aerosol profile with diffusion constants on the order of $D_a = 0.031$ and $D_b = 0.0083$. The inner electrode used in this measurement was found to be significantly bent. While holding each end in a lathe and rotating the electrode, the center of the electrode wobbled a distance of 0.64 mm. An electrode specially ground to be straighter wobbled only 0.13 mm and produced the profile in Figure 10b with diffusion constants of $D_a = 0.0073$ and $D_b = 0.0016$. Larger diffusion coefficients D_a indicate that there is more mixing of aerosol and sheath flow at smaller radii, i.e., closer to the inner electrode. The approximately five fold improvement in electrode straightness appears to be mirrored in a similar improvement in D_a, which represents mixing close to the inner electrode.

It was discovered that the acoustic excitation in the aerosol generation system produced a significant acoustic pulsation within the classifier. In addition, personal sampling pumps were used to recirculate the flow within the classifier that introduced additional pulsation within the classifier. These pulsations also produced large diffusion coefficients in the aerosol profiles similar to Figure 10a. When flow dampeners were introduced in line with the aerosol generator and pumps, an aerosol flow profile similar to that indicated in Figure 10b was produced. The fiber length coefficient of variation was also noticeably improved, but this improvement was not quantified.

This aerosol profile technique assesses only the flow characteristics of the classifier. Since the flow profile appears reasonably close to the ideal curve, it does not appear likely that the classifier flow characteristics are the principal cause of the observed broadening of the TEM length distribution under the best conditions currently achievable.

Electrical mobility technique

The measurement of electrical mobility of 0.8 μm latex particles resulted in the mobility distribution shown in Figure 11. The modes of the peaks agreed well with theoretical predictions of classifier penetration for 0.8 μm particles with the integral charge levels indicated; however, the peaks were approximately two times wider than predicted. This increase in width suggests that the electric field variation within the classifier was a major cause of length distribution broadening in the classified aerosol. This electric field variation may have been due to inaccuracy in machining of the classifier electrodes. It was difficult to obtain high accuracy and straightness in a rod over a 76 cm length. By special efforts in grinding the inner electrode, it was possible to achieve a maximum deviation of about 0.13 mm when rotating the rod while supporting the ends in a lathe. There were a number of regions of the entire classifier as indicated in Figure 1, all which had to be centered accurately to achieve good concentricity of the two electrodes in the classification region. We were not able to make direct measurements of electric field accuracy within the classifier. One parameter that provided an indication of electrode spacing was the classifier capacitance. Measurement of the capacitance while components of the classifier were rotated could indicate significant misalignment. The calculated capacitance of the two concentric tubes was 125 pF with a total measured classifier capacitance of 145 pF. In the current configuration, there was no significant

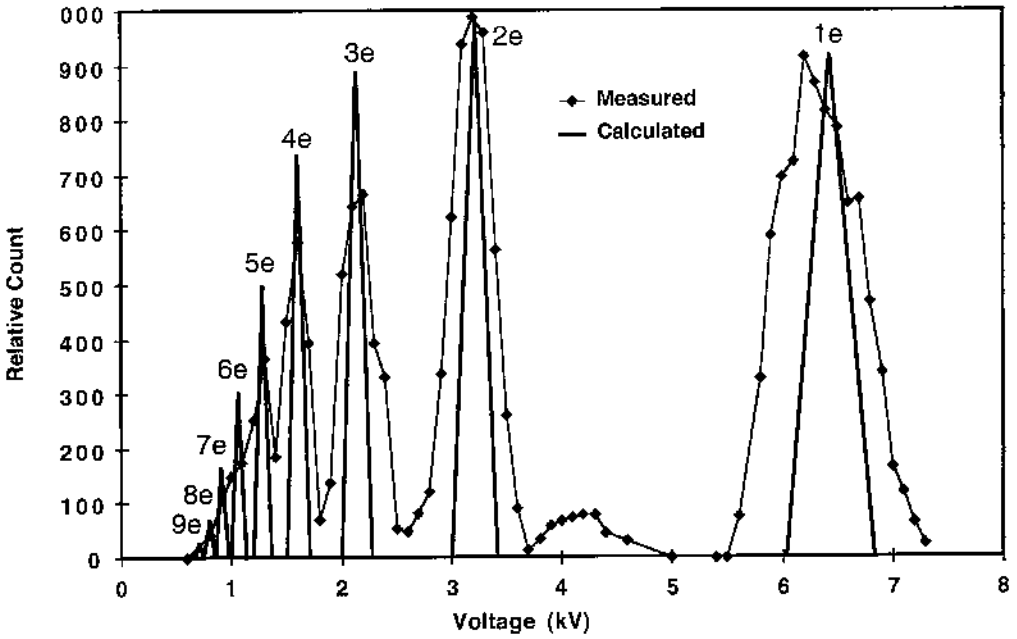

FIGURE 11. Calculated and measured mobilities of 0.8 μm latex particles with a Boltzmann charge distribution using the fiber length classifier as an electrical mobility classifier. The calculated distribution was normalized to have the same maximum height at the measured distribution. The peak at 4.2 kV is due to doublet particles.

change in capacitance with rotation of various components of the classifier. This did not appear to be a very sensitive indicator of misalignment.

COMPARISON OF EVALUATION TECHNIQUES

The measurement of fiber size distribution using the TEM provided the most accurate assessment of the fiber length classifier and must be carried out to calibrate the classifier. However, this accuracy, which comprises both bias and imprecision, comes at a price. To achieve reasonable precision, hundreds of fibers must be counted in each sample. Some biases in the measurement may enter the results due to sample preparation artifacts, e.g., fiber bundles are split apart, perhaps skewing the distribution. In addition to a day or two for sample preparation, TEM analysis of one sample takes days to complete, so feedback on the condition of the classifier can be slow. The split flow technique provides relatively rapid measurement of flow conditions within the classifier with results available in a period of hours. This technique does not provide information about misalignment of the electric field, though if the electrodes are misaligned or curved, some asymmetry in the flow field may result. However, this asymmetry due to electrode misalignment or curvature has not been directly documented. The measurement of spherical particle mobility is perhaps the quickest and most complete secondary check of classifier performance since it is a function of both the flow field and the electric field. However, it requires the insertion of a spacer to optimize flow conditions in the flow combination region; the use of this spacer may also be a source of flow disturbance. Placement of the spacer is a relatively minor inconvenience; the spacer must be

placed inside the flow combination region with the classifier disassembled. Only one peak in the mobility distribution needs to be measured to assess the resolution degradation within the system. A measurement of this type can be completed in less than an hour. Thus, the mobility measurement is the test of choice for evaluating the classifier. However, to separate the effect of flow field and electric field, the mobility measurement can be combined with the split flow measurement.

The fibers in this classifier are aligned perpendicularly to the direction of the air streamlines in the classification region. The fibers are therefore subject to a shear force due to the approximately parabolic flow profile. Preliminary estimates of the radial motion indicate that this motion is not significant compared to the dielectrophoretic force, but further calculations need to be carried out. It may also be that because many of the fibers are not ideal cylinders, the combined effect of alignment and shear flow may introduce a radial velocity component that increases the spread of the aerosol stream.

All observations indicate that some improvement in the classifier is possible. The current design was modeled after the inlet system in the Electrical Aerosol Analyzer (Model 3030, TSI, Inc., St. Paul, MN); perhaps improved flow accuracy would occur if the inner sheath flow starts from the top and the aerosol and outer sheath flows are combined successively from the periphery with the inner sheath flow as in the Differential Mobility Analyzer (Kinney et al. 1991; DMA, TSI, Inc.). Computer modeling of the DMA flow combination region has suggested some improvements in this approach (Chen and Pui 1997). Introduction of all of the flows at the top of the classifier would allow the smaller classified flow to be pulled into the inner electrode at the bottom (as in the DMA), rather than the current flow splitting arrangement. These modifications may reduce gravitational settling at the converging region of the current classifier and likely give a more precise split between classified flow and dump flow at the bottom. A more compact inlet design may also result in better alignment of the electrodes.

CONCLUSIONS

The fiber length classifier is the first classifier to accurately and predictably classify fibers according to length. CFD flow field calculations indicate that the flow field within the classifier should not result in reduced classifier accuracy. However, several types of measurement indicate that the classifier does not quite reach theoretical resolution. Three approaches to testing the classifier have been tried. The measurement of spherical particle electrical mobility seems the most promising routine check of classifier performance. However, microscope analysis of fiber lengths is necessary for calibration of the classifier. Once calibrated, the classifier appears to exhibit reliable performance and can be used to measure the length of aerosol fibers as well as produce monodisperse length fibers for other experiments. Work to improve the design of the classifier is continuing.

References

Baron, P. A. (1993). Measurement of Asbestos and Other Fibers. In *Aerosol Measurement: Principles, Techniques, and Applications*, edited by K. Willeke and P. A. Baron. Van Nostrand Reinhold, New York.

Baron, P. A., and Deye, G. J. (1990). Electrostatic Effects in Asbestos Sampling I: Experimental Measurements, *Am. Ind. Hyg. Assoc. J.* 51(2):51–62.

Baron, P. A., Deye, G. J., and Fernback, J. (1994). Length Separation of Fibers, *Aerosol Sci. Technol.* 21(2):179–192.

Baron, P. A., Deye, G. J., Fernback, J. E., and Jones, W. G. (1998). *Direct-Reading Measurement of Fiber Length/Diameter Distributions.* Advances in Environmental Measurement Methods for Asbestos, Boulder, CO, American Society for Testing Materials.

Blake, T., Jones, W., Schwegler-Berry, D., Baron, P., and Castranova, V. (1997). Effect of Fiber Length on Glass Microfiber Cytotoxicity, *Am. J. Respir. Critical Care Med.* 155:A959.

Burke, W. A., and Esmen, N. A. (1978). The Inertial Behavior of Fibers, *Amer. Ind. Hyg. Assoc. J.* 39:400–405.

Chen, B. T., Yeh, H. C., and Hobbs, C. H. (1993). Size Classification of Carbon Fiber Aerosols, *Aerosol Sci. Technol.* 19(2):109–120.

Chen, D. R., and Pui, D. Y. H. (1997). Numerical Modeling of the Performance of Differential Mobility Analyzers for Nanometer Aerosol Measurements, *J. Aerosol Sci.* 28(6):985–1004.

Griffiths, W. D. (1988). The Shape Selective Sampling of Fibrous Aerosols, *J. Aerosol Sci.* 19(6):703–713.

Han, R. J., Moss, O. R., and Wong, B. A. (1994). Airborne Fiber Separation by Electrophoresis and Dielectrophoresis: Theory and Design Considerations, *Aerosol Sci. Technol.* 21(3):241–258.

Hochrainer, D., Zebel, G., and Prodi, V. (1978). Ein gerät zur trennung von fasern und isometrischen partikeln bei der probenahme, *Staub-Reinhalt. Luft* 38(10):425–429.

Kasper, G. (1982). Dynamics and Measurement of Smokes. I. Size Characterization of Nonspherical Particles, *Aerosol Sci. Technol.* 1(2):187–200.

Kinney, P. D., Pui, D. Y. H., Mulholland, G. W., and Bryner, N. P. (1991). Use of the Electrostatic Classification Method to Size 0.1 μm SRM Particles–A Feasibility Study, *J. Res. Natl. Inst. Stand. Technol.* 96:147–176.

Lilienfeld, P. (1985). Rotational Electrodynamics of Airborne Fibers, *J. Aerosol Sci.* 16(4):315–322.

Lipowicz, P. J. (1994). *Theory of Fiber Length Separation by Combined Electrophoresis and Dielectrophoresis*. Fourth International Aerosol Conference, Los Angeles, CA.

Lipowicz, P. J., and Yeh, H. C. (1989). Fiber Dielectrophoresis, *Aerosol Sci. Technol.* 11(3):206–212.

Martonen, T. B. (1990). *Measurement of Aerodynamic Size and Related Risk of Airborne Fibers.* World Congress-Particle Technology, Kyoto Japan, Society of Powder Technology, Japan.

Spurny, K. R. (1980). Fiber Generation and Length Classification. In *Generation of Aerosols and Facilities for Exposure Experiments*, edited by K. Willeke. Ann Arbor Science Publishers, Ann Arbor, MI, pp. 257–298.

Stöber, W., Flachsbart, H., and Hochrainer, D. (1970). The Aerodynamic Diameter of Latex Aggregates and Asbestos Fibers, *Staub-Reinhalt. Luft* 30(7): 1–12.

Weyel, D. A., Ellakkani, M., Alarie, Y., and Karol, M. (1984). An Aerosol Generator for the Resuspension of Cotton Dust, *Toxic. and Appl. Pharmacology* 76:544–547.

White, F. M. (1986). *Fluid Mechanics*, McGraw-Hill, New York, p. 326.

Zebel, G., Hochrainer, D., and Boose, C. (1977). A Sampling Method with Separated Deposition of Airborne Fibres and Other Particles, *J. Aerosol Sci.* 8:205–213.

Received August 10, 1998; accepted November 25, 1998.